

Slow CCL2-dependent translocation of biopersistent particles from muscle to brain

Zakir Khan,^{1,2} Christophe Combadière,^{3,4,5} François-Jérôme Authier,^{1,2,6} Valérie Itier,^{1,2,11}
François Lux,^{7,8} Christopher Exley,⁹ Meriem Mahrouf-Yorgov,^{1,2,11} Xavier Decrouy,^{1,2}
Philippe Moretto,¹⁰ Olivier Tillement,^{7,8} Romain K. Gherardi^{1,2,6*} and Josette Cadusseau^{1,2,11*}

1 Inserm, U955, Créteil, 94000, France; **2** Université Paris Est, Faculté de Médecine, Créteil, 94000, France; **3** Inserm, U945-S, Paris, 75013, France; **4** Université Pierre et Marie Curie, Faculté de Médecine, Paris, 75013 France; **5** AP-HP, Groupe Hospitalier Pitié-Salpêtrière, Service d'Immunologie, Paris, 75013, France; **6** AP-HP, Hôpital H. Mondor - A. Chenevier, Service d'Histologie, Centre de Référence Neuromusculaire GNMH, Créteil, 94000, France; **7** CNRS UMR 5620, Laboratoire de Physico-Chimie des Matériaux Luminescents, Villeurbanne, 69622, France; **8** Université Claude Bernard Lyon 1, Villeurbanne, 69622, France ; **9** Keele University, The Birchall Centre, Lennard-Jones Laboratories, Staffordshire, ST5 5BG, UK; **10** CNRS UMR 5797, Centre d'Etudes Nucléaires de Bordeaux Gradignan, Gradignan, 33175, France, **11** Faculté des Sciences et Technologie, UPEC, Créteil, France.

* equal contribution

Zakir Khan, Inserm, U955, Créteil, 94000, France, Université Paris Est, Faculté de Médecine, Créteil, 94000, France: zakir.khan@pasteur.fr
Christophe Combadière, Inserm, U945-S, Paris, 75013, France; Université Pierre et Marie Curie, Faculté de Médecine, Paris, 75013 France; AP-HP, Groupe Hospitalier Pitié-Salpêtrière, Service d'Immunologie, Paris, 75013, France; : christophe.combadiere@upmc.fr

François-Jérôme Authier Inserm, U955, Créteil, 94000, France, Université Paris Est, Faculté de Médecine, Créteil, 94000, France, AP-HP, Hôpital H. Mondor - A. Chenevier, Service d'Histologie, Centre de Référence Neuromusculaire GNMH, Créteil, 94000, France : francois-jerome.authier@hmn.aphp.fr

Valérie Itier, Inserm, U955, Créteil, 94000, France, Université Paris Est, Faculté de Médecine, Créteil, 94000, France, Faculté des Sciences et Technologie, UPEC, Créteil, France: valerieitier@hotmail.com

François Lux, CNRS UMR 5620, Laboratoire de Physico-Chimie des Matériaux Luminescents, Villeurbanne, 69622, France; Université Claude Bernard Lyon 1, Villeurbanne, 69622, France : lux@pcml.univ-lyon1.fr

Christopher Exley, Keele University, The Birchall Centre, Lennard-Jones Laboratories, Staffordshire, ST5 5BG, UK : c.exley@chem.keele.ac.uk

Meriem Mahrouf-Yorgov, Inserm, U955, Créteil, 94000, France, Université Paris Est, Faculté de Médecine, Créteil, 94000, France, Faculté des Sciences et Technologie, UPEC, Créteil, France : meriem.yorgov@inserm.fr

Xavier Decrouy, U955, Créteil, 94000, France; Université Paris Est, Faculté de Médecine, Créteil, 94000, France : xavier.decrouy@inserm.fr

Philippe Moretto, CNRS UMR 5797, Centre d'Etudes Nucléaires de Bordeaux Gradignan, Gradignan, 33175, France : moretto@cenbg.in2p3.fr

Olivier Tillement, CNRS UMR 5620, Laboratoire de Physico-Chimie des Matériaux Luminescents, Villeurbanne, 69622, France; Université Claude Bernard Lyon 1, Villeurbanne, 69622, France : tillement@pcml.univ-lyon1.fr

Romain K. Gherardi, Inserm, U955, Créteil, 94000, France, Université Paris Est, Faculté de Médecine, Créteil, 94000, France, AP-HP, Hôpital H. Mondor - A. Chenevier, Service d'Histologie, Centre de Référence Neuromusculaire GNMH, Créteil, 94000, France : romain.gherardi@hmn.aphp.fr

Josette Cadusseau, Inserm, U955, Créteil, 94000, France, Université Paris Est, Faculté de Médecine, Créteil, 94000, France, Faculté des Sciences et Technologie, UPEC, Créteil, France josette.cadusseau@inserm.fr

corresponding authors: josette.cadusseau@inserm.fr; romain.gherardi@hmn.aphp.fr

Pr. Josette Cadusseau & Pr. Romain Gherardi

IMRB Team 10

8 rue du Général Sarrail

Faculté de Médecine

F-94010 France

Phone : 33 1 49 81 37 10

Fax : 33 1 49 81 37

ABSTRACT

Background : Long-term biodistribution of nanomaterials used in medicine is largely unknown. This is the case for alum, the most widely used vaccine adjuvant, which is a nanocrystalline compound spontaneously forming micron/submicron-sized agglomerates. Although generally well tolerated, alum is occasionally detected within monocyte-lineage cells long after immunization in presumably susceptible individuals with systemic/neurologic manifestations or autoimmune (inflammatory) syndrome induced by adjuvants (ASIA).

Methods : On the grounds of preliminary investigations in 252 patients with alum-associated ASIA showing both selective increase of circulating CCL2, the major monocyte chemoattractant, and a variation in the *CCL2* gene, we designed mouse experiments to assess biodistribution of vaccine-derived aluminium and of alum-particle fluorescent surrogates injected in muscle. Aluminium was detected in tissues by Morin stain and PIXE (Particle Induced Xray Emission). Both 500nm fluorescent latex beads and vaccine alum agglomerates-sized nanohybrids (Al-Rho) were used.

Results : Intramuscular injection of alum-containing vaccine was associated with appearance of aluminium deposits in distant organs such as spleen, and brain where they were still detected one year after injection. Both fluorescent materials injected into muscle translocated to draining lymph nodes (DLNs) and thereafter were detected associated with phagocytes in blood and spleen. Particles linearly accumulated in brain up to the 6-month endpoint, first found in perivascular CD11b⁺ cells and then in microglia and other neural cells. DLN ablation dramatically reduced the biodistribution. Cerebral translocation was not observed after direct intravenous injection, but significantly increased in mice with chronically altered blood-brain-barrier. Loss/gain-of-function experiments consistently implicated CCL2 in systemic diffusion of Al-Rho particles captured by monocyte-lineage cells, and in their subsequent neurodelivery. Stereotactic particle injection pointed out brain retention as a factor of progressive particle accumulation.

Conclusion : Nanomaterials can be transported by MO-lineage cells to DLNs, blood, and spleen, and, similarly to HIV, may use CCL2-dependent mechanisms to penetrate the brain. This occurs at very low rate in normal conditions explaining good overall tolerance of alum despite its strong neurotoxic potential. However, continuously escalating doses of this poorly biodegradable adjuvant in the population may become insidiously unsafe, especially in case of overimmunisation or immature/altered BBB or high constitutive CCL-2 production.

Key words :

alum
vaccine adverse effect
vaccine adjuvant
nanomaterial biodistribution
nanomaterial neurodelivery
macrophages
macrophagic myofasciitis
CCL-2
Single Nucleotide Polymorphisms (SNPs)

Background

Nanomaterials have various innovative medical applications including drug and gene delivery, imaging contrast fluids, topical antimicrobials, surgery tools and vaccines [1]. Due to the growing number of novel compounds and formulations, data on their specific biodistribution, persistence and toxicity are generally lacking [1], and clarification regarding how the body handles small particles, especially those which interact with immune cells [2], is urgently needed. Once defined, these basic mechanisms which govern host-particle interactions should be integrated with specific properties of nanomaterials (size, shape, surface, and solubility) to enable predictions of their beneficial or adverse effects.

The use of nanomaterials in Man is not as contemporary as is recently portrayed. For decades, alum, a nanocrystalline compound formed of aluminium oxyhydroxide, has been the most commonly used adjuvant in vaccines. The mechanism by which it stimulates the immune response is incompletely understood [3]. While alum is generally well tolerated, it is occasionally reported as the cause of disabling health problems in individuals with ill-defined susceptibility factors [4,5,6]. Clinical manifestations attributed to alum are paradigmatic of the so-called autoimmune/inflammatory syndrome induced by adjuvants (ASIA), a syndrome also observed in patients exposed to silicone gel [7]. They include delayed onset of diffuse myalgia [4], chronic fatigue [8], and stereotyped cognitive dysfunction [9]. The persistence of alum-loaded macrophages is typically detected at sites of previous injections (up to >12 years), resulting in a specific granuloma called macrophagic myofasciitis or MMF [4]. Although the biopersistence of adjuvants is *a priori* undesirable, the exact significance of this remains the subject of some debate since the biodistribution of slowly biodegradable particles following injection into muscle is currently unknown.

There appears to be a fine balance between the efficacy of alum adjuvant and its potential toxicity, and there is good evidence that these may be one and the same effect [3]. Both the efficacy and the potential toxicity of alum will be influenced by whether the bioactive nanomaterial remains localized at injection points or rather scatters and accumulates in distant organs and tissues. A reference study based on isotopic ^{26}Al showed poor (6%) ^{26}Al clearance in the urine at day 28 (d28) endpoint after i.m. injection of isotopic alum to rabbits, and detected ^{26}Al , in an unknown form, in lymph nodes, spleen, liver, and brain [10]. Aluminium oxyhydroxide is composed of micron/submicron-sized aggregates of nano-sized (ca 13 nm) particles and these aggregates were initially believed to remain extracellular until their complete solubilisation in interstitial fluids [10]. We now know that quite the reverse is the case and that antigen presenting cells (APCs) avidly take up alum particles

[11], and, in so-doing, become long-lived cells [12], and impede alum solubilisation [4,13,14]. Inflammatory monocytes (MOs) are attracted into muscle by danger signals through a monocyte chemoattractant protein-1 (MCP-1)/chemokine (C-C motif) ligand 2 (CCL2) driven-mechanism, becoming macrophages (MPs) and MO-derived dendritic cells (DCs), before migrating to the draining lymph nodes (DLNs) [15]. One function of migratory DCs is to transfer antigenic material to a large network of distant resident APCs [16]. Moreover, injections of alum alone induce significant changes linked to activation of the innate immune system in distant organs [17]. Therefore, we examined whether nanomaterials injected into muscle could translocate to distant organs as part of a general mechanism linked to phagocytosis and CCL2/MCP-1 signaling.

Methods

Mice models.

All animal experiments were conducted in accordance with the European guidelines for animal care. To facilitate mechanistic investigation of particle biodistribution, mice of the B57/B6 genetic background, that are used to generate genetically-manipulated models, were preferred to more toxic-sensitive mouse strains. Male 8-10 week-old C57BL/6, *mdx* (with leaky BBB), *CX3CR1*^{GFP/+} (with GFP reporter gene insertion allowing visualization of microglia), and *CCL2*^{-/-} mice were used (Jackson, West Grove, PA). Mice were protected from Al-containing materials, fed with manufactured animal food and water *ad libitum*, and exposed to 12:12 light/dark cycles. Experiments using fluorescent particles were extremely labour intensive and expensive to perform. All of them were done in triplicate. Homogeneity of results made unnecessary to use more than 3 mice per point.

Alum administration.

The dose of alum-containing vaccine administered to mice was calibrated to mimick the mean number of doses received by MMF patients. One dose of commercially available anti-hepatitis B vaccine contains 0.5mg Al according to the product data sheet. Based on an average of human body weight of 60kg (most patients being women), the amount received for each immunization is 8.33 μ g/kg. The allometric conversion from human to mouse (FDA Guidance 5541) gives a final amount of approximately 100 μ g/kg. 36 μ L vaccine, which corresponds to 18 μ g Al, was injected to mimick the cumulative effect induced by 5.2 human doses to 35g mice (the mean weight at the d180 midtime of brain analysis). This dose represents an equivalent 6.8 human doses in the youngest animal (27g body weight, 11 weeks of age at sacrifice) and 4.3 in the oldest one (42g at 62 weeks).

Furnace atomic absorption spectrometry.

Al concentrations were determined in whole TA muscles and brains dried at 37°C and digested with concentrated HNO₃ (14 mol/L). Digests were allowed to cool before dilution to 10% HNO₃ with ultra-pure water. The total aluminium in each digest was measured by THGA GFAAS, and results were expressed as Al mg/g tissue dry weight.

PIXE.

As in normal conditions Al may be detected with marked interindividual variations in tissues, *de novo* incorporation of aluminium in too low doses does not cause easily detectable changes when global conventional approaches are used [10]. Here we used PIXE, a procedure analysing radiations emitted from the interaction of a proton beam with the matter [19], to detect areas enclosing small Al spots. 20 μ m-thick sections

carefully protected from environmental Al were mounted on fresh formvar films, kept in the cryostat for 6h and stored under Al-free silica gel. Mineral and metal ions were detected using the nuclear microprobe of the Centre d'Etudes Nucléaires de Bordeaux-Gradignan. A 1MeV proton beam focused down to a 2 μ m spot was randomly scanned over multiple 500x500 μ m fields of tissue sections. In case of Al signal, re-test of 100x100 μ m areas of interest was performed. PIXE and Rutherford backscattering spectrometry analyses were employed simultaneously and quantitative results were computed, as previously described [19]. Al spots were considered eligible on 3 criteria: a size of more than 3 pixels (i.e. above the background noise), a depot not colocalized with Si, and a depot surrounded by a rounded halo of decreased intensity (both characteristics limiting confusion with contamination by external dust overcoming the protection procedures).

Synthesis of Al-Rho particles.

Gadolinium oxide nanohybrids with Al(OH)₃ coating were obtained in three steps: (i) gadolinium oxide nanoparticles were first synthesized, (ii) polysiloxane shell growth was then induced by hydrolysis-condensation of convenient silane precursors in presence of the nanoparticles, and (iii) the nanohybrids were coated by the addition of aluminium nitrate and soda in stoichiometric conditions.

Chemicals.

Gadolinium chloride hexahydrate ([GdCl₃, 6H₂O], 99.99%), sodium hydroxide (NaOH, 99.99%), tetraethyl orthosilicate (Si(OC₂H₅)₄, TEOS, 98%), (3-aminopropyl) triethoxysilane (H₂N(CH₂)₃-Si(OC₂H₅)₃, APTES, 99%), triethylamine (TEA, 99.5%), Rhodamine B Isothiocyanate (RBITC), Aluminium Nitrate Nonahydrate (Al(NO₃)₃.9H₂O, ACS reagent \geq 98%) and dimethyl sulfoxide (DMSO, 99.5%) were purchased from Sigma-Aldrich (St Louis, MO). Diethylene glycol (DEG, 99%) was purchased from SDS Carlo Erba (France).

Preparation of Gadolinium Oxide Core.

A first solution was prepared by dissolving [GdCl₃, 6H₂O] (0.56g) in 50mL DEG at room temperature. A second solution was prepared by adding a NaOH solution (0.49mL, 10M) in 50mL DEG. The second solution was progressively added to the first one, at room temperature, for 15 hours. A transparent colloid of gadolinium oxide nanoparticles in DEG was obtained.

Encapsulation of Gd₂O₃ cores by Polysiloxane Shell.

105 μ L of APTES and 67 μ L of TEOS were added to the 100mL of the gadolinium oxide nanoparticle solution under stirring at 40°C. 5 μ L of APTES was previously coupled to 1mg RBITC in DMSO (1mL) used as solvent and then added to the colloidal solution. After 1h, 1913 μ L of a DEG solution (0.1M of TEA, 10M of water) was

added. The whole coating procedure was repeated three more times (with no more addition of RBITC), every 24h. The final mixture was stirred for 48h at 40°C. The obtained solution could be stored at room temperature for weeks without alteration.

Coating of fluorescent nanohybrids with a Al(OH)₃ shell.

2.5mL of the colloidal solution was diluted by 2 to obtain a 5mL solution in DEG. 75mg of aluminium nitrate nonahydrate was dissolved in 10mL of water before addition to the colloidal solution. The resulting mixture was stirred for 5min and 4mL of a soda solution (0.2M) was added before stirring for 1hour.

Purification.

Purification of Al-Rho was performed by tangential filtration through Vivaspin filtration membranes (MWCO=10kDa) purchased from Sartorius Stedim Biotech (France). The colloidal solution was introduced into 20mL Vivaspin tubes, and centrifuged at 4100rpm. This step was repeated several times, by filling the tubes with water and centrifuging again, until the desired purification rate was reached (≥ 100). The purified colloidal solution was freeze dried for storage in 5 pillboxes, using a Christ Alpha 1-2 lyophilisator. The compound contained 4 μ g Al per μ L of Al-Rho suspension. Control transmission electron microscopy showed non-fibrous particles sizing about 10nm typical of aluminium hydroxyde (traditional precipitated alum). Similarly to vaccine alum, they formed agglomerates of submicronic /micronic size. Immunological properties of such traditional alum-protein precipitates are quite similar to those of the reference adjuvant approved by FDA (Al oxyhydroxyde : Alhydrogel®) and differ from other formulations not licensed for human use (18).

Peripheral injections of fluorescent nanomaterials.

Two types of fluorescent nanomaterials were used: exploratory polychromatic FLBs (500nm fluorospheres, Polysciences, PA), and confirmatory Al-Rho nanohybrids constructed with a rhodamine containing core and an Al(OH)₃ shell. FLBs were used first because they offer several characteristics that facilitate their detection in tissues, including strong fluorescence, spheric appearance and homogeneous size. This allowed us to get clear picture of what was happening in terms of biodistribution of these avidly phagocytized particles. Al Rho particles were less fluorescent, and more heterogeneous in shape and size than FLBs but represented better alum adjuvant surrogates. Almost all biodistribution experiments performed with FLBs in WT mice were also done with Al-Rho. In contrast FLBs and Al Rho were differentially used in mutated/genetically-modified mice: FLBs were preferred to study particle biodistribution in *mdx* mice with BBB alterations and when the GFP marker was used (i.e. *CX3CR1*^{GFP/+} mice with fluorescent microglia, GFP+ BMT studies); Al-Rho particles were

preferred in gain/loss of CCL2/MCP-1 function studies designed on the basis of preliminary results on the CCL2 status of alum-intolerant humans.

FLB suspension diluted at 1:1 in PBS contained $1.8 \cdot 10^{11}$ particles per mL. A total volume of 40 μ L (20 μ L in each TA muscle) was injected, corresponding to a total amount of $7.2 \cdot 10^9$ particles. The same volume of Al-Rho suspension was injected in TA muscles. PBS-injected mice were used as controls. Tissues including popliteal and inguinal DLNs, spleen, brain and blood were collected at various time points post injection. Three mice (n=3) were included per group at each time point for both injected materials and their controls. Other administration routes were compared to the standard i.m. injection, including s.c. injection of 20 μ L FLBs in each hindlimb, and i.v. injection of 40 μ L FLBs in the tail vein.

Stereotactic cerebral injections.

Mice were anaesthetized with ketamine and xylazine. Al-Rho suspension (0.5 μ L) was stereotactically injected in the striatum using a 1 μ L Hamilton syringe. Biodistribution of i.c. injected Al-Rho to cervical DLNs, assessed by serial sectioning of the whole cervical region, and spleen, was compared to biodistribution to popliteal DLN and spleen of the same amount of Al-Rho injected in TA muscle.

Pharmacological and physical migration blockade.

The prostaglandin analog BW245C, an agonist of PGD2 receptor, was used to inhibit APC migration as previously reported [20]. Since BW-245C is active for 2 days after injection, BW245C (100nM, Cat.no.12050, Cayman Chemical, MI, USA) was injected twice in TA muscle: it was first co-injected with FLBs at d0 and a second time alone at d2, DLNs being removed for examination at d4. Untreated FLB-injected mice were used as controls. In another set of experiments DLNs were surgically ablated, and mice immediately injected with FLBs in TA muscle.

Loss and gain of CCL2 function experiments.

Exploratory analyses performed in MMF patients with ASIA (see supplementary information section) yielded a CCL2 signal in form of (1) selective increase of CCL2 in the serum of MMF patients compared to healthy controls, and (2) a given haplotype in the *CCL2* gene tending to be more frequent in MMF patients than in the general population. These results incited us to use mouse models to explore the role of CCL2 in the biodisposition of particulate materials. Loss of CCL2 function studies were done using *CCL2*^{-/-} mice injected i.m. with 40 μ L Al-Rho. Gain of CCL2 function experiments consisted first in i.m. co-injection of 10 μ L murine rCCL2 (100 μ g/ml; R&D, MN) with 40 μ L Al-Rho. DLNs were removed at d4, spleen, brain and blood at d21. In other

experiments murine rCCL2 was infused into brain through a catheter stereotactically inserted into the striatum at d7 post-Al-Rho, fed by a subcutaneously implanted osmotic micropump fixed into the neck (0.25 μ L/h Alzet brain infusion kit, Charles River, France). rCCL2 was infused during 14 days (diffusion rate 180pg/day), with or without rCCL2 i.m. injection concurrent with Al-Rho injection. At d21 post Al-Rho injection, animals were sacrificed, and blood and tissues were collected. For controls, osmotic pumps filled with PBS were used.

Tissue preparation and particle counting.

Mice under terminal anaesthesia were transcardially perfused with PBS followed by ice-cold 4% paraformaldehyde (PFA) in 0.1M phosphate buffer. Tissues and organs were removed, post-fixed in PFA for 4 hours at 4°C, immersed overnight at 4°C in a 30% sucrose solution, and quickly frozen. Whole brains were serially cut into coronal cryosections of 40 μ m, spleen and muscle into 20 μ m, and DLNs into 10 μ m, and stored at -20°C until particle counting or treatment. Brain sections were successively deposited on 10 different Superfrost® slides in order to obtain 10 identical series, thus allowing determination of total particle content by multiplying by 10 the number of particles found in one series. A similar approach was used for DLNs and spleen. Blood was collected by heart puncture and 100 μ L were smeared for particle counting.

Immunohistochemistry and Morin staining.

Immunostaining was done using commercial primary antibodies routinely used in the lab, raised against CD11b (1/200, AbD Serotec, Oxford, UK), F4/80 (1/50, AbCam, Cambridge, UK), GFAP (1/200, DakoCytomation, France), vimentin (1/500 DakoCytomation, Trappes, France), collagen IV (1/100 Millipore, Temecula, CA), NG2 (1/200, Millipore, Molsheim, France), MAP2 (1/100, Sigma-Aldrich, Lyon, France), and IL1 β (1/100, AbCam, Paris, France) or nonspecific mouse IgG (Jackson ImmunoResearch, Suffolk, UK). Then, biotinylated anti-rat and anti-rabbit antibodies (1/200, Vector Laboratories, Paris, France) were used accordingly, and revealed using Alexa fluor 488-conjugated streptavidin (1/200 Invitrogen, Cergy-Pontoise, France). Neuron labeling was done using NeuroTrace® blue fluorescent Nissl Stain according to the manufacturer (Invitrogen). Al was stained with Morin (M4008-2G, Sigma-Aldrich) used as 0.2g dissolved in a solution consisting of 0.5% acetic acid in 85% ethanol [21]. Formation of a fluorescent complex with Al was detected under a 420nm excitation wavelength as an intense green fluorescence with a characteristic 520nm emission. Notably nanohybrids (Gd_2O_3) core encapsulated by polysiloxane shell were not positively stained by Morin. In contrast, when coated with Al(OH)₃, these particles were strongly positive for Morin. Fluorescence microscopy and spectral analyses were done using Carl Zeiss light and confocal microscopes.

Cell isolation from blood and tissues and flow cytometry.

For blood cell immunophenotyping, 100µL blood was treated with EDTA and stained with FITC-conjugated antibodies. Erythrocytes were lysed using hypotonic lysis solution, and then cells were washed with DMEM and sorted using a MoFlo cell sorter (Beckman Coulter, Villepinte, France). Cells were extracted from tissues of exsanguinated mice perfused with PBS. Tissues were removed and freshly dissociated in DMEM. DLTs and spleen were dissociated in DMEM containing 0.2% collagenase-B (Roche Diagnostics, Meylan, France) and 0.2% trypsin-EDTA at 37°C for 45 min twice. Brain tissue was dissociated in 1% Trypsin-HBSS (Thermo Scientific HyClone, South Logan, UK) containing 100U/mL DNase (Roche Diagnostics). Cell suspension were filtered and counted. CD45⁺ or CD11b⁺ cells were isolated using magnetic cell sorting (MACS, Miltenyi Biotec, Paris, France) and stained with one of the following antibodies and their isotypes: fluorescein isothiocyanate FITC-conjugated anti-CD11b, FITC-conjugated anti-Ly-6C (GR1), FITC-conjugated anti-CD11c (BD-Pharmingen Bioscience, San Diego, CA). Cells were sorted using a cell sorter. Populations presenting >90% purity were used. Sorted cells were cytospined and stained with Hoechst-33342 for nucleus. Particle loaded cells were counted under fluorescence microscope.

BM transplantation experiments.

GFP⁺ BM cells were obtained by flushing the femurs of adult CAG-GFP mice and injected retroorbitally (1×10^7 cells per mouse) to 4-week-old C57BL/6 mice, as previously described [15]. Recipient mice were irradiated at 9.0Gy on day1 before transplantation, and were treated with 10mg/kg/day ciprofloxacin for 10 days. Blood chimaerism of >90% was controlled at 3–4 weeks post-transplantation.

Statistical analyses.

All experimental values are presented as means and standard deviation except when indicated. Statistical analyses used unpaired Student's *t*-test (genotypes), *p* <0.05 was considered significant.

Results

Intramuscular alum-containing vaccine injection in mouse induces Al deposition in distant tissues

Alum-containing vaccine (36µL corresponding to 18µg Al) was first injected in the *tibialis anterior* (TA) muscles of C57Bl6 mice. It induced an acute inflammatory reaction which stabilized after d4 in the form of collections of typical alum-loaded MPs with large hematoxylin⁺ and Periodic Acid Schiff⁺ cytoplasm in muscle envelopes (Fig. 1 a). In parallel, the local Al tissue concentration determined by atomic absorption spectrometry decreased by 50% from injection to d4 and then remained stable until d21 (2342, 1122, and 1180 µg/g of dry muscle tissue,

respectively). Al was additionally located in muscle and distant tissues by particle induced X-ray emission (PIXE) [19]. Random scanning of 20 μ m thick sections, sampled and processed with careful protection against environmental Al, disclosed significant Al signals in muscle, spleen and brain (Fig. 1 b-c). In brain, Al spots accounted for 38, 21, and 37 % of 500x500 μ m tested fields at d21, month 6 and 12 (mo6 and mo12) post-injection, respectively (mean=31.5%; n=73 fields, Fig. 1 d). The dip at month 6, was either due to interindividual variations in aluminium handling or to sampling problems related to variable proportions of grey and white matter in the randomly scanned areas (see below). The spot size ranged from about 1 to 14 μ m. By comparison, 5 unvaccinated mice showed only 7 positive out of 94 tested fields (mean=7.4%). These results confirmed that Al derived from alum can be translocated to, penetrate and persist in brain tissue [21,22,23]. Al depots detected in spleen and brain could have resulted from either physical translocation of alum particles, or *in situ* aggregation of soluble Al, or both.

Fluorospheres injected into mouse muscle undergo lymphatic and systemic biodistribution

To examine if particles translocate to distant sites, we next injected polychromatic fluorescent latex beads (FLBs). A size of 500nm was chosen as an approximate of the average size of alum agglomerates observed *in vivo*, allowing FLB visualization as individual spheres by confocal and fluorescence microscopes (resolution > 200nm). After i.m. injection of 20 μ L suspensions, FLBs transiently peaked in free form in blood (1200+400 FLBs per 100 μ L) at h1. As early as 1h post-injection, some FLBs had also reached DLNs. I.m. injection of GFP⁺CD45⁺ cells, either pre-loaded with FLBs or coinjected with FLBs, showed no GFP⁺ cells translocation to DLNs at h1 (data not shown), indicating early cell-independent particle translocation to DLNs by lymphatic drainage of the muscle interstitial fluid [24]. In DLNs, however, most FLBs were cell-associated suggesting rapid capture by DLN resident cells. Within 24h, FLBs were phagocytized by muscle CD11b⁺ MO/MPs. Phagocytes progressively cleared the particles away from the interstitium to form collections (Fig. 2a), mainly located in muscle envelopes at d4.

At d4, FLBs had dramatically increased in DLNs, forming intracellular agglomerates in interfollicular area (Fig. 2 b-e). Particle-loaded cells extracted from DLNs at d4 were CD45⁺, CD11b⁺, and more often GR1⁺/Ly6C⁺ (69-81%), and CD11c⁺, with either intermediate (46%) or high (22%) intensity (Fig. 2a,c,d), thus corresponding to MO-derived inflammatoty DCs and MPs [25]. Co-injection of FLBs with the synthetic prostaglandin analog BW245C, a compound known to inhibit DC migration [20], inhibited FLB translocation to DLNs at d4, by 32% in the popliteal and 69% in inguinal DLNs, respectively (Fig. 2f). This indicated prominent particle transport within

phagocytic cells, at least downstream to popliteal DLN. At later time points, both the number of particle-loaded cells and the individual cell load markedly decreased in DLNs (Fig. 2e). While decreasing in DLNs, FLBs dramatically increased in spleen from d4 to d21 (Fig. 3 a,b). As spleen is unplugged to lymphatic vessels, the particle transfer from DLNs to spleen implicated exit from the lymphatic system through the thoracic duct and circulation in the blood stream. Consistently, smears showed similar d21 peak of FLB-loaded CD11b⁺ cells in the circulation (Fig. 3 c,d). From d4, circulating FLBs were cell-associated (Fig. 3 d). Most FLB-loaded cells in blood, DLNs and spleen exhibited a few particles and were GR1⁺/Ly6C⁺ (Fig 3 ef). However, 22-33% were GR1⁻/Ly6C⁻ in spleen and had frequently incorporated >5FLBs, suggesting phagocytosis-associated maturation of inflammatory MO-derived cells [20,25,26]. FLB-loaded cells had markedly decreased in spleen at d90. Although declining after d21, FLB-loaded cells were still detected in blood at d45 and d90.

Fluorosphere incorporation into brain is delayed and depends on prior cell loading in peripheral and lymphoid tissues

Particles were detected in brain mainly from d21 post-injection. After d21 post-i.m. injection, FLBs gradually increased in brain until the d90 endpoint in the C57Bl6 mouse (Fig. 4 a,b) and until the d180 endpoint in the CX3CR1^{GFP/+} mouse conventionally used to study resident microglia (Fig. 4 a, 5a). FLBs were predominantly found in the grey matter (82-95%), regardless of the amount of injected FLBs (4, 10, 20µL), vaccine co-injection (36µL), or post-injection time from d21 to d365. Some FLBs were detected in leptomeninges (9%) and in the white matter (9%) at d21, but these locations became rare at later time points. FLBs were <5% in choroid plexus (table1). Comparative FLB distribution at mo3, mo6 and mo12 showed no prominent accumulations of particles at any neuroanatomical location (Fig. 4c). FLBs were usually detected in brain as single particles located within or at the surface of cells; 37-62% of particles could be reliably assigned to a given cell subset by immunohistochemical screening. At d21, particles were mainly associated with perivascular CD11b⁺ MPs, but at d90 they were also found in deep ramified CX3CR1⁺microglia (Fig. 5 a). Particles were also detected in GFAP⁺ astrocytes, MAP2⁺ or Neurotrace-stained neurons, and vimentin⁺ leptomeningeal cells (Fig. 5 b-e), and in NG2⁺ oligodendroglial progenitors/pericytes (not shown). FLB incorporation into GFP⁺ resident ramified microglia of CX3CR1^{GFP/+} mice increased by up to 26-fold the d21 value at d180.

Importantly, compared to i.m. injection, the same FLB amount injected in the tail vein resulted in virtually no cerebral entry at d21 and d90 in C57Bl6 mice (Fig. 6 a). Moreover, ablation of popliteal and inguinal DLNs

before FLB injection in TA muscle resulted in 60-80% reduction of FLB incorporation into blood, spleen and brain compartments at d21 (Fig. 6 b). Thus, cell uptake in muscle and DLNs, and subsequent cell traffic to blood crucially contributed to delayed particle translocation to spleen and brain (Fig. 6 a-f). Consistently, by injecting FLBs into muscle of GFP⁺bone marrow (BM) chimaeric mice obtained by transplanting GFP⁺BM-derived cells to irradiated syngenic C56Bl/6 mice [15], we detected FLB-loaded GFP⁺cells in these organs (Fig. 7 a,b,c), and observed delayed incorporation of donor-derived cells in brain (Fig. 7 d,e).

This BM transplantation model is known to be associated with irradiation-induced blood-brain barrier (BBB) alteration. Dystrophin-deficient *mdx* mice also have chronically altered BBB [27]. As a corollary, compared to age-matched controls, they show significantly more CD31⁺ brain capillaries, and dramatic increase of perivascular CD11b⁺ macrophages (Fig. 6c) at the expense of deep ramified microglia. FLB injection in *mdx* mouse muscle resulted in increased brain incorporation of particles at both d21 and d90, as assessed by both histology and cytopspins of CD45⁺/CD11b⁺cells extracted from brain (Fig. 6 d,e,f). Thus, BBB alteration and/or the associated inflammatory/angiogenic response likely favours brain incorporation of circulating particle-loaded cells.

Fluorescent nanohybrids coated with Al(OH)₃ undergo CCL2-dependent systemic scattering and brain penetration

For confirmatory experiments we constructed fluorescent particles mimicking alum. Rhodamine nanohybrids [28] were covalently coated with a Al(OH)₃ shell. As assessed by the Morin stain for aluminium, these Al-Rho particles were avidly phagocytosed after i.m. injection and formed intracellular agglomerates similar in size to the vaccine adjuvant (Fig. 8 a,b). Biodistribution of the alum fluorescent surrogate injected into TA muscle was strikingly similar to that of FLB (table 2), including d4 peak in DLNs, d21 peak in spleen, delayed entry in brain, and main association with GR1⁺/Ly6C⁺ MOs in tissues (Fig. 8 c-h). Compared to i.m. injection, subcutaneous injection of Al-Rho particles was associated with even higher rate of diffusion to DLNs (Fig. 8 f), a finding consistent with the presence of abundant migratory DCs in skin.

On the grounds of the human SNP study, we performed CCL2 gain and loss of function experiments to investigate the role of CCL2-responsive cells in particle scattering and neurodelivery. Injection of Al-Rho particles into the TA muscle of CCL2-deficient mice decreased particle incorporation by 35% into popliteal DLN and by 76% in inguinal DLN at d4, and by 71%, 85% and 82% in spleen, blood, and brain, respectively, at d21 (Fig. 9 a). Conversely, Al-Rho particle biodistribution increased in different gain of CCL2 function experiments

(Fig. 9 b-d). I.m. co-injection of Al-Rho with murine recombinant CCL2 (rCCL2: 1 μ g) increased particle incorporation by 47% into popliteal and 163% into inguinal DLN (d4), and by 180% in spleen, 274% in blood, and 341% in brain (d21).

Moreover, slow intracerebral (i.c.) infusion of CCL2 by an osmotic pump (180 pg/day during 15 days starting at d7 after Al-Rho i.m. injection) increased by 74% particle incorporation into brain at d21 compared to PBS control. Combination of i.m. injection and i.c. infusion of rCCL2 increased particle incorporation into brain by 539%. Despite important interindividual variations, a consistent trend of CCL2-dependent increase of Al brain levels was detected 21 days after i.m. injection of 40 μ L of alum-containing vaccine (Fig. 9 e). Taken together these results indicate that after i.m. injection, particles associated with inflammatory MOs can enter the brain using a CCL2-dependent mechanism, possibly through a Trojan horse mechanism. Importantly, Al-Rho particles gaining access to the brain after i.m. injection remained intact since they were still coated with Al(OH)₃ as assessed by both Morin stain (Fig. 10 a), and PIXE (Fig. 10 b). Their incorporation in neural cells was consistently associated with expression of IL-1 β (Fig. 10 c), a reliable marker of particle-induced NALP3 inflammasome activation [29].

Fluorescent nanohybrids coated with Al(OH)₃ are retained in brain

An apparently irreversible accumulation of nanomaterials after i.m. injection was unique to brain tissue which lacks conventional lymphatic pathways and may retain immune cells [30]. We stereotactically injected 0.5 μ L Al-Rho in the striatum of C57BL/6 mice, and counted particles in cervical LNs, blood, and spleen at d4 and d21. Compared to the same amount of Al-Rho injected in the TA muscle, i.c. injection was associated with almost no particle translocation to regional DLNs (Fig. 10 d), and appearance of 8-fold less particles in spleen (Fig. 10 e). Since 25 free Al-Rho particles per 100 μ L were detected in blood at h1, it is likely that the rare particles subsequently detected in spleen reflected direct particle passage into blood during i.c. injection. It seems therefore that lack of recirculation likely contributed to progressive cerebral particle accumulation.

Discussion

Particles injected by the i.m. or s.c. route gained access to distant tissues. Latex and Al-Rho particles showed closely similar biodistribution, suggesting a shared basic scattering mechanism. Initial cell uptake in peripheral and DLN tissues and subsequent transport within inflammatory MO-derived cells was critically involved, as indicated by immunophenotyping, cell migration blockade and DLN ablation. Cells were heavily loaded with particles soon after i.m. injection but usually contained only 1–2 particles after d4 and downstream the

popliteal DLN, pointing to either dilution by cell division [31] or particle dispatching to other cells [32] within DLNs. Previous studies have reported particle cell transport from skin to DLNs [25] but downstream particle fate remained largely unexplored [33]. There is strong evidence that, in inflammatory conditions, all DCs reaching DLNs do not die locally but may rather gain access to the blood through efferent lymphatics and the thoracic duct, and present antigens in spleen and bone marrow [33]. Ingested adjuvant particles boost this phenomenon which in turn likely favours their translocation from the injection point to distant sites as: (i) alum induces rapid differentiation of monocyte-lineage cells into APCs [34], and stimulates their migration to DLNs [35], (ii) beryllium hydroxide, a closely similar particulate adjuvant, strongly stimulates DC egress through efferent lymphatics [36], and, as shown herein, (iii) Al deposits may be detected by PIXE in spleen and brain after i.m. injection of alum.

Delayed and slowly progressive particle accumulation occurred in intact brains. Experiments using the parabiosis model [37] or avoiding brain irradiation prior to BM transplantation [38] have shown that endogenous microglia are not replenished by the periphery under normal CNS conditions. Although low chimerism inherent to these experimental approaches may lead to some underestimation of slow microglia turnover from the periphery [39], a more likely explanation of our findings is that particles exert stimulatory effects on myeloid cell trafficking [36]. Both latex particles and aluminium hydroxide agglomerates promote inflammation [40,41] and non-specific immune stimulation can increase by up to 20-fold monocyte transendothelial migration in *in vitro* models of the BBB [42]. Consistently, i.m. injection of rCCL2 strongly increased particle incorporation into intact brain while CCL2-deficient mice had decreased neurodelivery. rCCL2 likely induced the exit of inflammatory MOs and hematopoietic stem and progenitor cells from BM [43], followed by their transmigration to the injected muscle and to DLNs [44], prior to particle loading and dissemination. Cerebral infusion of low doses of rCCL2, mimicking pathologic states attracting inflammatory monocytes, also increased particle neurodelivery. Intracerebral particles translocated with time from perivascular macrophages to the sentinel network of parenchymal microglia and to other resident neural cells, and likely failed to recirculate, thus explaining their progressive cerebral accumulation.

Conclusion.

Taken together, our results indicate that, similarly to intracellular bacteria [45], nanomaterials can be transported by MO-lineage cells to DLNs, blood, and spleen, and, similarly to HIV [46] and other pathogens [47], may use CCL2-dependent MO transmigration across the BBB to enter the brain. This occurs at extremely

low rate in normal mice, the percentage of injected particles found in tissues being estimated at 1:10⁵ in d21 spleen and 1:10⁷ in d90 brain, consistently with the excellent tolerance of almost all individuals to limited doses of alum and other injected particles. Neurodelivery of nanomaterials significantly increased in mice with either weak BBB or high tissue levels of CCL2, as previously suspected for pathogens in humans [48]. On the one hand, such a cerebral incorporation of nanomaterials injected into tissues should be regarded as an interesting characteristic in the setting of therapeutic strategies targeting the CNS. On the other hand alum has high neurotoxic potential [49], and planning administration of continuously escalating doses of this poorly biodegradable adjuvant in the population should be carefully evaluated by regulatory agencies since the compound may be insidiously unsafe. It is likely that good tolerance to alum may be challenged by a variety of factors including overimmunization, BBB immaturity, individual susceptibility factors, and ageing that may be associated with both subtle BBB alterations and progressive increase of CCL2 production (50).

Abbreviations :

Al-Rho: Al(OH)3 rhodamine nanohybrid; ASIA: autoimmune/inflammatory syndrome induced by adjuvant; BBB: blood brain barrier; CCL2: chemokine (C-C motif) ligand 2; CNS: central nervous system; d: day; FLB: fluorescent latex bead; *mdx* : dystrophin deficient mouse; MCP1: monocyte chemoattractive protein 1; MMF: macrophagic myofasciitis; MO: monocyte; mo: month; MP: macrophage; PIXE: proton induced X-ray emission; SNP: single nucleotide polymorphism; TA: tibialis anterior muscle.

Competing interest :

The authors declare no conflict of interest.

Authors contribution

Z.K. carried out animal experiments and tissue processing and participated to data analysis; C.C. carried out molecular genetics studies; F.J.A. contributed clinical data; V.I. processed tissue for PIXE and participated to their analysis; F.L. participated to surrogate particles production; C.E. carried out Al determination in tissues; M.M.Y. and P.M participated to the PIXE analysis, X.D carried out confocal analysis; O.T. conceived and contributed surrogate particles; R.K.G. conceived and coordinated the study, analyzed data and drafted the manuscript; J.C. designed the study; performed animal experiments, analyzed data and prepared the figures, participated in the manuscript writing. All authors read and approved the manuscript.

Acknowledgement

This work has benefited from research funding from two patients associations: E3M (Entraide aux Malades de Myofasciite à Macrophages) "Neurodélivrance des particules injectées par voie intra musculaire et sécurité des adjuvants aluminiques", AFM (Association Française contre les Myopathies) "Etude des mécanismes de la myofasciite à macrophages" and Dwoskin Foundation (Nano in brain); from Région Ile-de-France through a programme PICRI (Partenariat Institutions-Citoyens pour la Recherche et l'Innovation) "Recherche de polymorphismes dans les gènes codant pour des facteurs inflammatoires (chimiokines) dans la myofasciite à macrophages", and through two post-doctoral positions from NeRF (Neuropole de Recherche Francilien) on the topic "The macrophage as a Trojan horse for brain delivery" and "Brain delivery of i.m. injected nanoparticles : relevance to safety of aluminium-containing adjuvants of vaccines"; and from the European Community's Seventh Framework Programme in the project ENDOSTEM "Activation of vasculature associated stem cells and muscle stem cells for the repair and maintenance of muscle tissue" (Grant agreement number 241440). We would like to thank for their most useful contributions : Dr Sophie Hue, Dr Fabrice Chrétien, Dr Madly Brigitte, Dr Anne Hulin, Lucie Poupel, Emilie House, Yasmine Baba-Amer, and Mathieu Surenaud.

REFERENCES

- [1] Committees on toxicity, mutagenicity and carcinogenicity of chemicals in food, consumer products and the environment (COT, COM, COC). Joint statement on nanomaterial toxicology, December 2005. Available at <http://www.food.gov.uk/multimedia/pdfs/cotstatements2005nanomats.pdf>.
- [2] Dobrovolskaia MA, Aggarwal P, Hall JB, McNeil SE. Preclinical studies to understand nanoparticle interaction with the immune system and its potential effects on nanoparticle biodistribution. *Mol Pharm* 2008;5:487-495.
- [3] Exley C, Siesjö P, Eriksson H. The immunobiology of aluminium adjuvants: how do they really work? *Trends Immunol* 2010;31:103-109.
- [4] Gherardi RK, Coquet M, Cherin P, Belec L, Moretto P, Dreyfus PA, Pelissier JF, Chariot P, Authier FJ. Macrophagic myofasciitis lesions assess long-term persistence of vaccine-derived aluminium hydroxide in muscle. *Brain* 2001;124:1821-1831.
- [5] Authier FJ, Cherin P, Creange A, Bonnotte B, Ferrer X, Abdelmoumni A, Ranoux D, Pelletier J, Figarella-Branger D, Granel B, Maisonneuve T, Coquet M, Degos JD, Gherardi RK. Central nervous system disease in patients with macrophagic myofasciitis. *Brain* 2001;124:974-983.
- [6] Gherardi RK, Authier FJ. Aluminum inclusion macrophagic myofasciitis: a recently identified condition. *Immunol Allergy Clin North Am* 2003;23:699-712.
- [7] Shoenfeld Y, Agmon-Levin N. 'ASIA' Autoimmune/inflammatory syndrome induced by adjuvants. *J Autoimmunity* 2010;36:4-8.
- [8] Authier FJ, Sauvat S, Champey J, Drogou I, Coquet M, Gherardi RK. Chronic fatigue syndrome in patients with macrophagic myofasciitis. *Arthritis Rheum* 2003;48:569-570.
- [9] Couette M, Boisse MF, Maison P, Brugieres P, Cesaro P, Chevalier X, Gherardi RK, Bachoud-Levi AC, Authier FJ. Long-term persistence of vaccine-derived aluminum hydroxide is associated with chronic cognitive dysfunction. *J Inorg Biochem* 2009;103:1571-1578.
- [10] Flarend RE, Hem SL, White JL, Elmore D, Suckow MA, Rudy AC, Dandashli EA. In vivo absorption of aluminium-containing vaccine adjuvants using 26Al. *Vaccine* 1997;15:1314-1318.
- [11] Morefield GL, Sokolovska A, Jiang D, HogenEsch H, Robinson JP, Hem SL. Role of aluminum-containing adjuvants in antigen internalization by dendritic cells in vitro. *Vaccine* 2005;23:1588-1595.
- [12] Hamilton JA, Byrne R, Whitty G. Particulate adjuvants can induce macrophage survival, DNA synthesis, and a synergistic, proliferative response to GM-CSF and CSF-1. *J Leukoc Biol* 2000;67:226-232.
- [13] Verdier F, Burnett R, Michelet-Habchi C, Moretto P, Fievet-Groyne F, Sauzeat E. Aluminium assay and evaluation of the local reaction at several time points after intramuscular administration of aluminium containing vaccines in the Cynomolgus monkey. *Vaccine* 2005;23:1359-1367.
- [14] Authier FJ, Sauvat S, Christov C, Chariot P, Raisbeck G, Poron MF, Yiou F, Gherardi R. AlOH3-adjuvanted vaccine-induced macrophagic myofasciitis in rats is influenced by the genetic background. *Neuromuscul Disord* 2006;16:347-352.

- [15] Brigitte M, Schilte C, Plonquet A, Baba-Amer Y, Henri A, Charlier C, Tajbakhsh S, Albert M, Gherardi RK, Chrétien F. Muscle resident macrophages control the immune cell reaction in a mouse model of notexin-induced myoinjury. *Arthritis Rheum* 2010;62:268-279.
- [16] Carbone FR, Belz GT, Heath WR. Transfer of antigen between migrating and lymph node-resident DCs in peripheral T-cell tolerance and immunity. *Trend Immunol* 2004;25:655-658.
- [17] Wang XY, Yao X, Wan YM, Wang B, Xu JQ, Wen YM. Responses to multiple injections with alum alone compared to injections with alum adsorbed to proteins in mice. *Immunol Lett* 2012;149:88-92.
- [18] Cain DW, Sanders SE, Cunningham MM, Kelsoe G. Disparate adjuvant properties among three formulations of "alum". *Vaccine*. 2013;31:653-660.
- [19] Moretto P. Nuclear microprobe: a microanalytical technique in biology. *Cell Mol. Biol.* 1996; 42:1-16.
- [20] Wen GY, Wisniewski HM. Histochemical localization of aluminum in the rabbit CNS. *Acta Neuropathol* 1985;68:175-184.
- [21] Redhead K, Quinlan GJ, Das RG, Gutteridge JM. Aluminium-adjuvanted vaccines transiently increase aluminium levels in murine brain tissue. *Pharmacol Toxicol* 1992;70:278-280.
- [22] Sahin G, I Varol, A Temizer, K Benli, R Demirdamar, S Duru. Determination of aluminum levels in the kidney, liver, and brain of mice treated with aluminium hydroxide. *Biol. Trace Elem Res* 1994;41:129-135.
- [23] Kivelä R, M. Silvennoinen, M. Lehti, H. Kainulainen, Vihko V. Effects of acute exercise, exercise training, and diabetes on the expression of lymphangiogenic growth factors and lymphatic vessels in skeletal muscle. *Am. J. Physiol. Heart Circ Physiol* 2007;293:H2573-H259.
- [24] Randolph GJ, Inaba K, Robbiani DF, Steinman RM, Muller WA. Differentiation of phagocytic monocytes into lymph node dendritic cells in vivo. *Immunity* 1999;11:753-761.
- [25] Allan RS, Waithman J, Bedoui S, Jones CM, Villadangos JA , Zhan Y, Lew AM, Shortman K, Heath WR, Carbone FR. Migratory dendritic cells transfer antigen to a lymph node-resident dendritic cell population for efficient CTL priming. *Immunity* 2006;25:153-162.
- [26] Arnold L, Henry A, Poron F, Baba-Amer Y, van Rooijen N, Plonquet A, Gherardi RK, Chazaud B. Inflammatory monocytes recruited after skeletal muscle injury switch into antiinflammatory macrophages to support myogenesis. *J Exp Med* 2007;204:1057-1069.
- [27] Nico B, Frigeri A, Nicchia GP, Corsi P, Ribatti D, Quondamatteo F, Herken R, Girolamo F, Marzullo A, Svelto M, Roncali L. Severe alterations of endothelial and glial cells in the blood-brain barrier of dystrophic mdx mice. *Glia* 2003;42, 235-251.
- [28] Fizet J, Rivière C, Bridot L, Charvet N, Louis C, Billotey C, Racourt M, Morel G, Roux S, Perriat P, Tillement O. Multi-luminescent hybrid gadolinium oxide nanoparticles as potential cell labeling. *J Nanosci Nanotechnol* 2009;9:5717-5725.
- [29] Hornung V, Bauernfeind F, Halle A, Samstad EO, Kono H, Rock KL, Fitzgerald KA, Latz E. Silica crystals and aluminum salts activate the NALP3 inflammasome through phagosomal destabilization. *Nat Immunol* 2008;9,847-56.
- [30] Weller RO, Djuanda E, Yow HY, Carare RO. Lymphatic drainage of the brain and the pathophysiology of neurological disease. *Acta Neuropathol* 2009;117:1-14.

- [31] Kabashima K, Banks TA, Ansel KM, Lu TT, Ware CF, Cyster JG. Intrinsic lymphotoxin-beta receptor requirement for homeostasis of lymphoid tissue dendritic cells. *Immunity* 2005;22:439-450.
- [32] Angeli V, Ginhoux F, Llodrà J, Quemeneur L, Frenette PS, Skobe M, Jessberger R, Merad M, Randolph GJ. B cell-driven lymphangiogenesis in inflamed lymph nodes enhances dendritic cell mobilization. *Immunity* 2006;24:203-215.
- [33] Cavanagh LL, Bonasio R, Mazo IB, Halin C, Cheng G, van der Velden AW, Cariappa A, Chase C, Russell P, Starnbach MN, Koni PA, Pillai S, Weninger W, von Andrian UH. Activation of bone marrow-resident memory T cells by circulating antigen-bearing dendritic cells. *Nat Immunol* 2005;6:1029-1037.
- [34] Rimaniol AC, Gras G, Verdier F, Capel VB, Grigoriev F, Porcheray E, Sauzeat JG, Fournier P, Clayette CA, Siegrist D, Dormont. Aluminum hydroxide adjuvant induces macrophage differentiation towards a specialized antigen-presenting cell type. *Vaccine* 2004;22:3127-3135.
- [35] Kool M, Soullié T, van Nimwegen M, Willart MA, Muskens F, Jung S, Hoogsteden HC, Hammad H, Lambrecht BN. Alum adjuvant boosts adaptive immunity by inducing uric acid and activating inflammatory dendritic cells. *J Exp Med* 2008;205:869-882.
- [36] Hall JG. Studies on the adjuvant action of beryllium. I. Effects on individual lymph nodes. *Immunology* 1998;53:105-113.
- [37] Ajami B, Bennett JL, Krieger C, Tetzlaff W, Rossi FM. Local self-renewal can sustain CNS microglia maintenance and function throughout adult life. *Nat Neurosci* 2007; 10:1538-1543.
- [38] Mildner A, Schmidt H, Nitsche M, Merkler D, Hanisch UK, Mack M, Heikenwalder M, Brück W, Priller J, Prinz M. Microglia in the adult brain arise from Ly-6C^{hi}CCR2⁺ monocytes only under defined conditions. *Nat Neurosci* 2007;10:1544-1553.
- [39] Prinz M, Mildner A. Microglia in the CNS: immigrants from another world. *Glia* 2011;59:177-187
- [40] Inoue K, Takano H, Yanagisawa R, Koike E, Shimada A. Size effects of latex nanomaterials on lung inflammation in mice. *Toxicol Appl Pharmacol* 2009;234:68-76.
- [41] Pauluhn J. Pulmonary toxicity and fate of agglomerated 10 and 40 nm aluminium oxyhydroxides following 4-week inhalation exposure of rats: toxic effects are determined by agglomerated, not primary particle size. *Toxicol Sci* 2009;109:152-167.
- [42] Persidsky Y, Stins M, Way D, Witte MH, Weinand M, Kim KS, Bock P, Gendelman HE, Fiala M. A model for monocyte migration through the blood-brain barrier during HIV-1 encephalitis. *J Immunol* 1997;158, 3499-3510.
- [43] Si Y, Tsou CL, Croft K, Charo IF. CCR2 mediates hematopoietic stem and progenitor cell trafficking to sites of inflammation in mice. *J Clin Invest* 2010;120:1192-1203.
- [44] Palframan RT, Jung S, Cheng G, Weninger W, Luo Y, Dorf M, Littman DR, Rollins BJ, Zweerink H, Rot A, von Andrian UH. Inflammatory chemokine transport and presentation in HEV: a remote control mechanism for monocyte recruitment to lymph nodes in inflamed tissues. *J Exp Med* 2001;5:1361-1373.
- [45] Chackerian AA, Alt JM, Perera TV, Dascher CC, Behar SM. Dissemination of *Mycobacterium tuberculosis* is influenced by host factors and precedes the initiation of T-cell immunity. *Infect Immun* 2002;70:4501-4509.

- [46] Drevets DA, MJ Dillon, JS Schawang, N Van Rooijen, J Ehrchen, C Sunderkötter, PJ Leenen. The Ly-6Chigh monocyte subpopulation transports *Listeria monocytogenes* into the brain during systemic infection of mice. *J Immunol* 2004;172:4418-4424.
- [47] Eugenin EA, Osiecki K, Lopez L, Goldstein H, Calderon TM, Berman JW. CCL2/monocyte chemoattractant protein-1 mediates enhanced transmigration of human immunodeficiency virus (HIV)-infected leukocytes across the blood-brain barrier: a potential mechanism of HIV-CNS invasion and NeuroAIDS. *J Neurosci* 2006;26:1098-1106.
- [48] Gonzalez E, Rovin BH, Sen L, Cooke G, Dhanda R, Mummidi S, Kulkarni H, Bamshad MJ, Telles V, Anderson SA, Walter EA, Stephan KT, Deucher M, Mangano A, Bologna R, Ahuja SS, Dolan MJ, Ahuja SK. HIV-1 infection and AIDS dementia are influenced by a mutant MCP-1 allele linked to increased monocyte infiltration of tissues and MCP-1 levels. *Proc Natl Acad Sci USA* 2002;99:13795-13800.
- [49] Shaw CA, Petrik MSJ. Aluminum hydroxide injections lead to motor deficits and motor neuron degeneration. *J Inorg Biochem* 2009;103:1555-1562.
- [50] Galimberti D, Fenoglio C, Lovati C, Venturelli E, Guidi I, Corr`a B, Scalabrini D, Clerici F, Mariani C, Bresolin N, Scarpini E. Serum MCP-1 levels are increased in mild cognitive impairment and mild Alzheimer's disease. *Neurobiol Aging* 2006 ; 27 : 1763-8.

Legends of the figures**Figure 1 : Aluminium deposits in tissues following injection of alum-containing vaccine in the TA muscle.**

- a-** Granuloma composed of PAS⁺ cells is formed in the injected muscle envelope;
- b-** PIXE mapping shows muscle Al deposits in pseudocolors, with confirmatory Al emission spectrum (d21);
- c-** Section of spleen tissue (left panel) displays the large 500x500µm and restricted 100x100µm protonized fields corresponding to the PIXE maps (middle and right panel, respectively) enclosing eligible Al spots (d21);
- d-** Section of brain tissue (left left panel) displays the restricted 100x100µm protonized field corresponding to the PIXE map (middle panel) enclosing eligible Al spot (d21); the number or fields containing one or more Al spots were increased at all tested time points compared to unvaccinated (right panel) mice. (bars: 100µm).

Figure 2 : FLB translocation in DLN following injection in TA muscle.

- a-** Marked translocation of FLBs in parafollicular areas of popliteal DLNs (d4);
 - b-** Flow cytometry showing that most FLB-loaded cells extracted from DLN express CD11c at either an intermediate or strong level (d4);
 - c-** Immunocytochemistry on CD11b⁺ cells extracted from DLNs were usually Gr1⁺/Ly6C⁺, especially when they had ingested a few particles (left), whereas heavily loaded ones were often Gr1⁻/Ly6C⁻ (right);
 - d-** The number of FLB-loaded cells peaked at d4 post-injection in both popliteal and inguinal DLNs;
 - e-** The migration inhibitor BW245C co-injected with FLBs in muscle markedly decreased the number of FLB-loaded cells detected in DLNs at d4 post-injection. The effect was more pronounced in the downstream inguinal DLN;
 - f-** The migration inhibitor BW245C co-injected with FLBs in muscle markedly decreased the number of FLB-loaded cells detected in DLNs at d4 post-injection. The effect was more pronounced in the downstream inguinal DLN;
- (histograms : n=3 per group, mean +SD, * p<0.05, ** p<0.01, *** p<0.005; bars: 100µm [a]; 5µm [c]).

Figure 3 : FLB biodistribution in spleen and blood following injection in TA muscle.

- a-** The number of FLB-loaded cells peaked at d21 in spleen;
- b-** In spleen, FLBs were detected in CD11b⁺ cells as assessed by immunohistochemistry (left) or after cell sorting (right);
- c-** On blood smears, most FLBs were cell-associated from d4, and peaked at d21 post injection; Circulating FLB-loaded cells were still detected at d90 endpoint;
- d-** Circulating FLB-loaded cells were CD11b⁺ (d21);

e,f- GR1/Ly6C immunophenotyping of CD11b⁺ cells that have ingested FLBs. Most are Gr1⁺/Ly6C⁺ both in DLNs at d4 (a) and spleen at d21 (b).
 (histograms n=3 per group, mean±SD, * p<0.05, ** p<0.01, *** p<0.005; bars : 5 μm).

Figure 4 Brain translocation of FLBs following injection in TA.

- a-** Cerebral translocation of FLBs was delayed but relentless until the D90 endpoint in C57 mice and the D180 endpoint in the CX3CR1^{GFP/+} mouse;
- b-** Unstained section of the brainstem in a C57 mouse at d21 post-injection showing FLBs mostly distributed in the subpial region;
- c-** FLBs distribution in the brain: areas enriched in FLBs were reported on semi-serial rostro-caudal sections of mouse brain stained by Cresyl violet (A to G), using dots of different colors according to the considered time point (d21 to d365) after i.m. injection. Report was done regardless of the number of enclosed particles in each selected area. Note that FLBs were always predominantly found in the grey matter without prominent accumulations at any specific neuroanatomical site.

(histograms : n=3 per group, mean +SD, * p<0.05, ** p<0.01, *** p<0.005; bar in b: 50μm).

Figure 5 : FLBs in various neural cells.

- a-** Unstained section of the brain parenchyma of a CX3CR1^{GFP/+} mouse at d90 post-injection showing individual FLBs in a significant proportion of GFP⁺ ramified microglial cells;
- b-e-** In brain of C57 mice at d21post-injection, FLBs were detected in F4/80⁺ perivascular macrophages(b), GFAP⁺ astrocytes (c), neurotrace®⁺ neurons (d), and vimentin⁺ pial cells (e);
 (bars: 10μm).

Figure 6 : mechanisms of FLBs translocation.

- a-** Compared to the i.m. route, direct injection of FLBs in the tail vein of C57 mice was associated with almost no brain translocation at both d21 and d90 post-injection;
- b-** Popliteal and inguinal DLN ablation was associated with marked decrease of FLB-loaded cells in blood, spleen and brain at d21 post-injection;
- c-** The *mdx* mouse with altered BBB showed marked increase of the perivascular CD11b⁺ cell population, and significant angiogenesis assessed by an increase of CD31⁺ endothelial cells, compared to normal C57 mice;
- d-e-** *Mdx* mice showed increased incorporation of FLBs in brain; compared to C57 mice, *mdx* mice had increased FLB neurodelivery at both d21 and d90, as assessed by both histology (d) or after CD11b⁺ cell sorting (e);
- f-** At d21, FLBs were mainly detected outside capillary basement membranes immunostained for collagenIV (upper pannel), closely associated with CD11b⁺ perivascular macrophages (lower pannel);

(histograms : n=3 per group, mean +SD, * p<0.05, ** p<0.01, *** p<0.005; bar in d: 10μm).

Figure 7 : GFP⁺ BM chimeric mice.

a-c Chimeric mice injected intramuscularly with FLBs showed GFP+ BM-derived cells enclosing FLBs among inflammatory cells extracted from the injected muscle (a) at d4 after FLB injection, in spleen (b) and brain (c) at d33 after FLB injection.

d-e Chimeric mice showed incorporation of GFP+ cells in the brain, mainly in form of perivascular cells in the cortex (d), and occasionally in more deeply located ramified CD11b+ cells (e, arrow) at d180 post-BM transplantation.

(bars: 10μm)

Figure 8 : Biodistribution of Al particles.

a- Morin stain for aluminium shows rounded alum cytoplasmic agglomerates within muscle macrophages after i.m. vaccine administration in C57 mouse;

b- Morin stain confirms that phagocytized Al-Rho nanohybrids are associated with Al and form particles similar in size to alum agglomerates;

c-e- Al-Rho nanohybrids show time-dependent distribution in DLNs, spleen, and brain strikingly similar to that of FLBs;

f- Al-Rho injected by the s.c. route translocate to DLNs and spleen, as observed with the i.m. route;

g,h- Ly6C immunophenotyping of CD11b⁺ cells that have ingested Al-Rho : most are Gr1⁺/Ly6C⁺ both in DLNs at d4 (g) and spleen at d21 (h).

(histograms : n=3 per group, mean ± SD, * p<0.05, ** p<0.01, *** p<0.005; bar in a: 10μm).

Figure 9 : CCL2-dependent systemic translocation of Al-particles:

a- CCL2 deficient mice show dramatic decrease of Al-Rho translocation from the injected muscle to inguinal DLN, blood, spleen and brain, as compared to their respective controls (100%). Note that difference is significant but less pronounced for popliteal DLN;

b- rCCL-2 co-injection with Al-Rho is associated with marked increase of Al-Rho translocation from the injected muscle to inguinal DLN, blood, spleen and brain, compared to their respective controls (100%). Note that difference is significant but less pronounced for popliteal DLN;

c- rCCL-2 infused by an osmotic micropump into the striatum for 15 days is associated with significant increase of Al-Rho translocation from the injected muscle to brain;

d- Combined i.m. and i.c. injection of rCCL2 is associated with dramatic increase of FLB translocation from muscle to both blood and brain;

e- Alum-containing vaccine injected into muscle of CCL-2-deficient, normal, and rCCL-2 mice was associated with a trend of CCL-2-dependent increase of Al concentration levels in brain;

(histograms : n=3 per group, mean ± SD, * p<0.05, ** p<0.01, *** p<0.005, except [e]: n=10 per group, mean ± SEM).

Figure 10 : Al-Rho particles remain in brain and may induce inflammation.

- a-** Al-Rho nanomaterial detected in brain by rhodamine fluorescence (upper row and emission spectrum at 560nm) remains associated with Al as assessed by Morin stain (middle row and emission spectrum at 520nm);
- b-** Al-Rho nanomaterial detected in brain by PIXE. Al coating colocalizing with Gd core assesses the integrity of Al-Rho nanohybrid after translocation;
- c-** In mice with i.m. co-injection of Al-Rho and rCCL-2, particle incorporation into neural cells was associated with immunohistochemical expression of IL1beta;
- d-** Stereotactic injection of Al-Rho into the striatum was associated with no translocation to cervical LNs (CLN) at d4, contrasting with conspicuous translocation to popliteal LNs (PLN) observed when the same particle amount was injected in TA muscle;
- e-** Stereotactic injection of Al-Rho into the striatum, compared to similar injection into muscle, was associated with very little translocation to spleen at both d4 and d21.;
- (histograms : n=3 per group, mean \pm SD, * p<0.05, ** p<0.01, *** p<0.005; bar in c: 10 μ m).

Table 1 : distribution of particles (percent of total) according to post-injection time.

Localization	Time post-injection			
	D21	D90	D180	D365
Choroid plexus	0%	5%	5%	3%
Leptomeninges	9%	5%	0%	3%
Parenchyma	91%	90%	95%	94%

Table 2 : time of peak observation and peak value of particles loaded cells in studied organs (total number \pm SD).

Particle	Popliteal DLN		Inguinal DLN		Spleen		Blood		Brain	
	peak	Nb of loaded cells	peak	Nb of loaded cells	peak	Nb of loaded cells	peak	Nb of loaded cells	endpoint	Nb of loaded cells
FLB	D4	21 117 \pm 1 235	D4	23 746 \pm 2 880	D21	76 503 \pm 11 850	D21	9878 \pm 792	D90	577 \pm 96
Al-Rho	D4	4 462 \pm 257	D4	6 253 \pm 745	D21	27 570 \pm 6 670	D21	7546 \pm 1034	D90	613 \pm 137

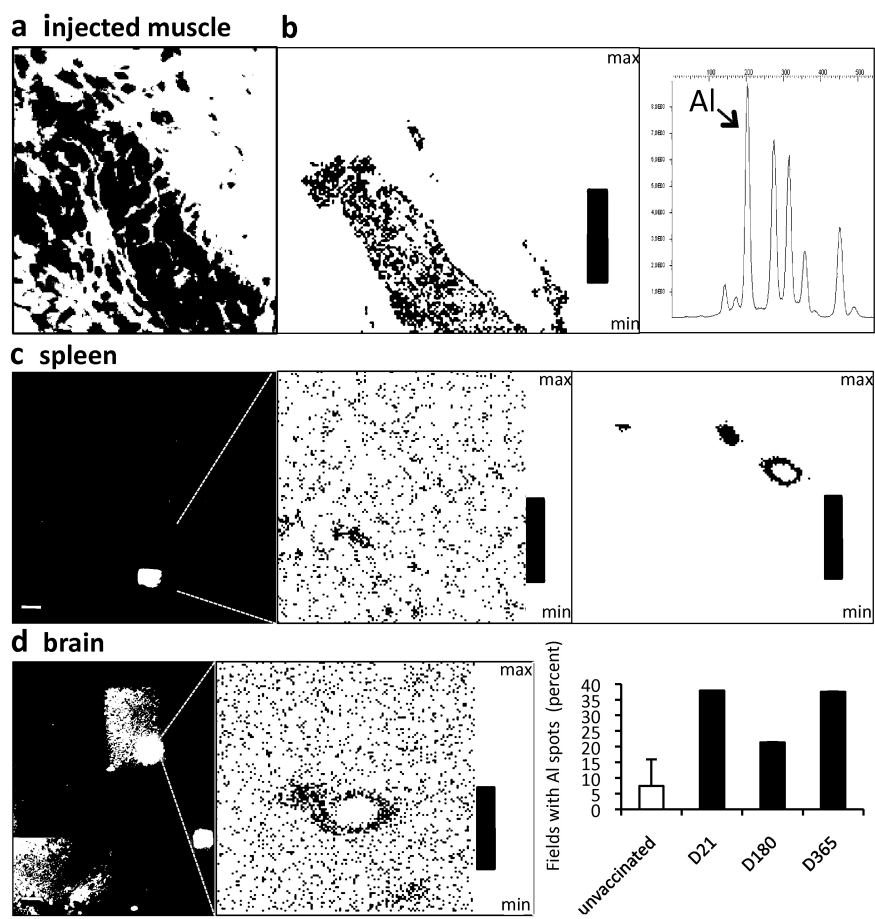


Figure 1

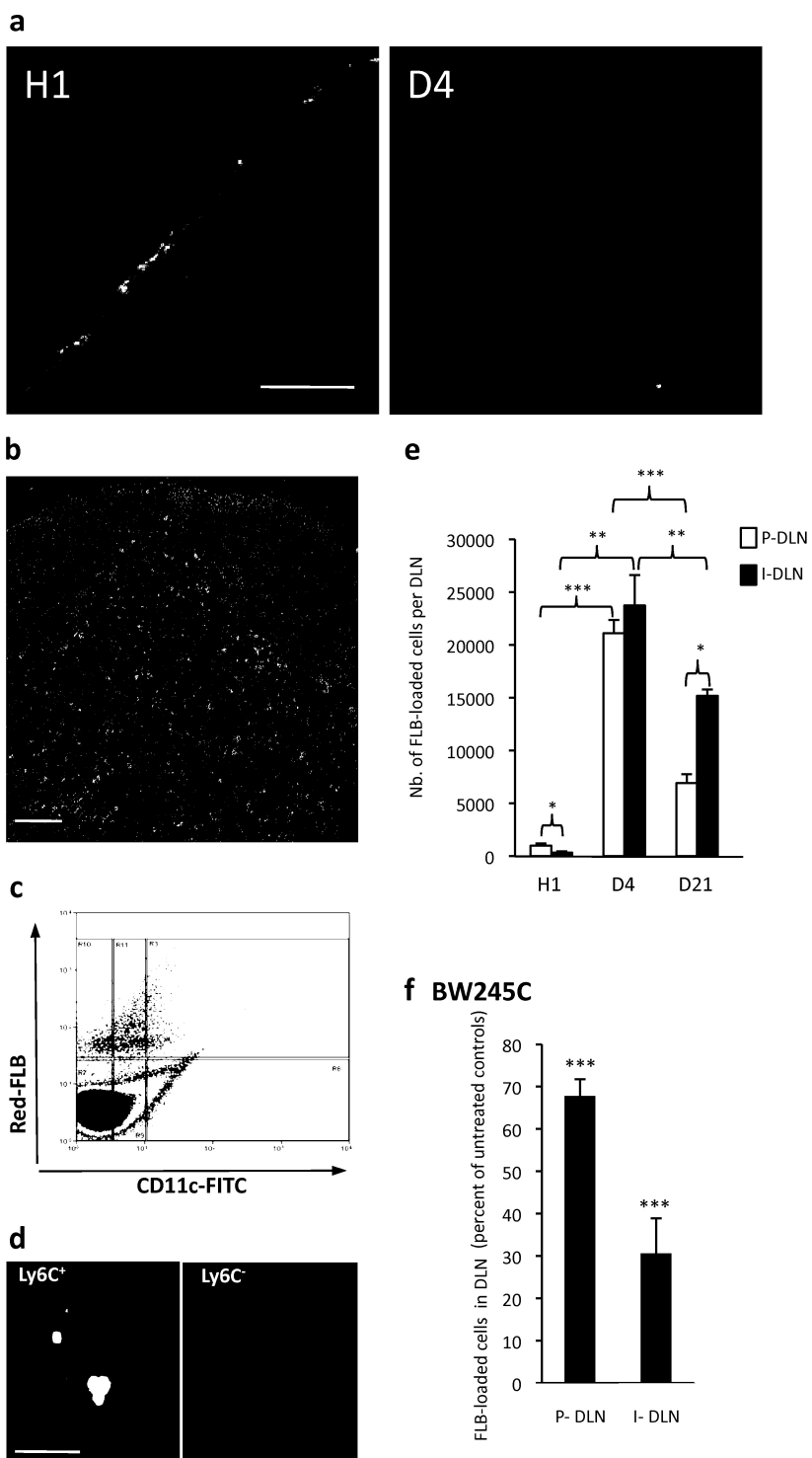


Figure 2

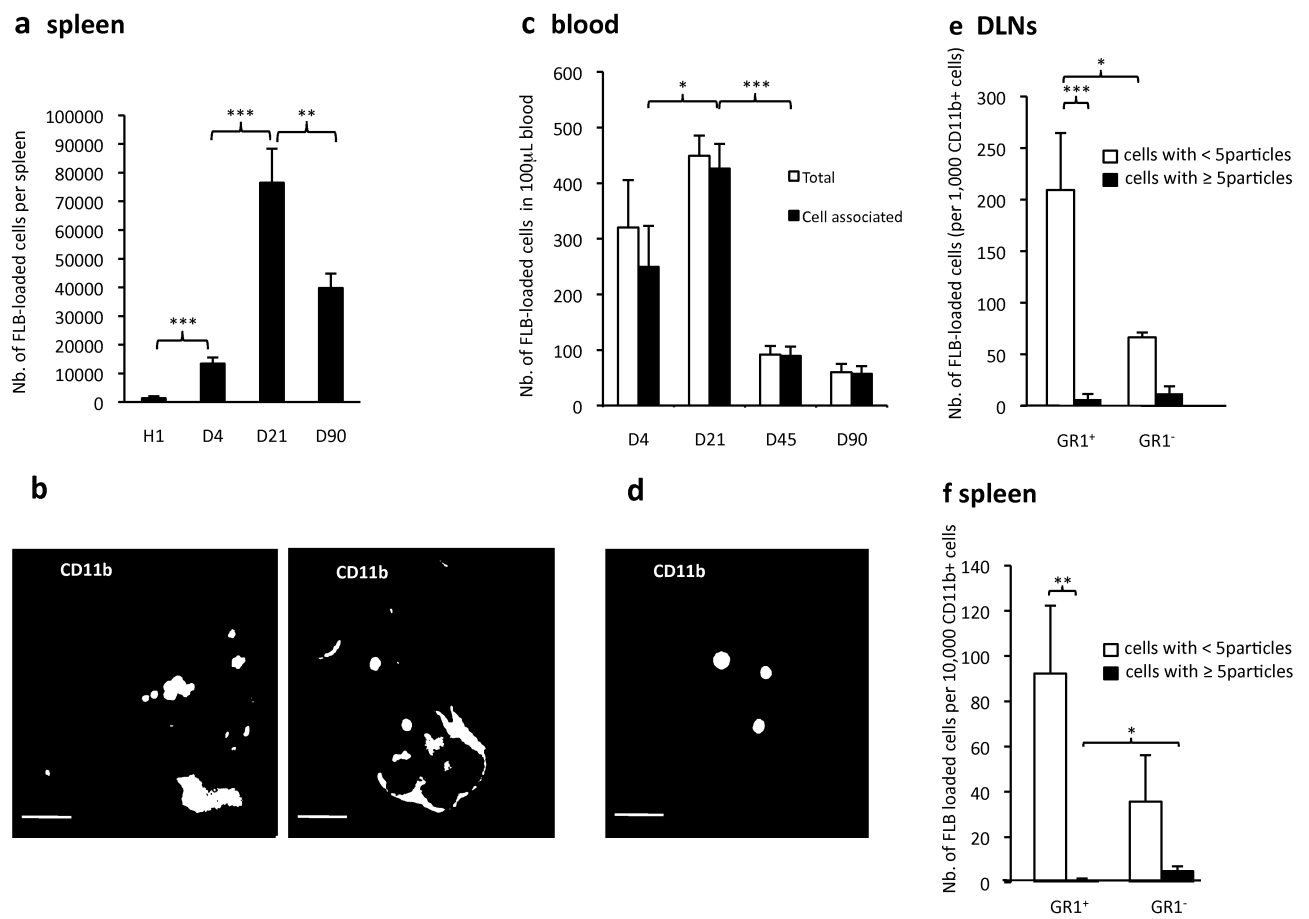


Figure 3

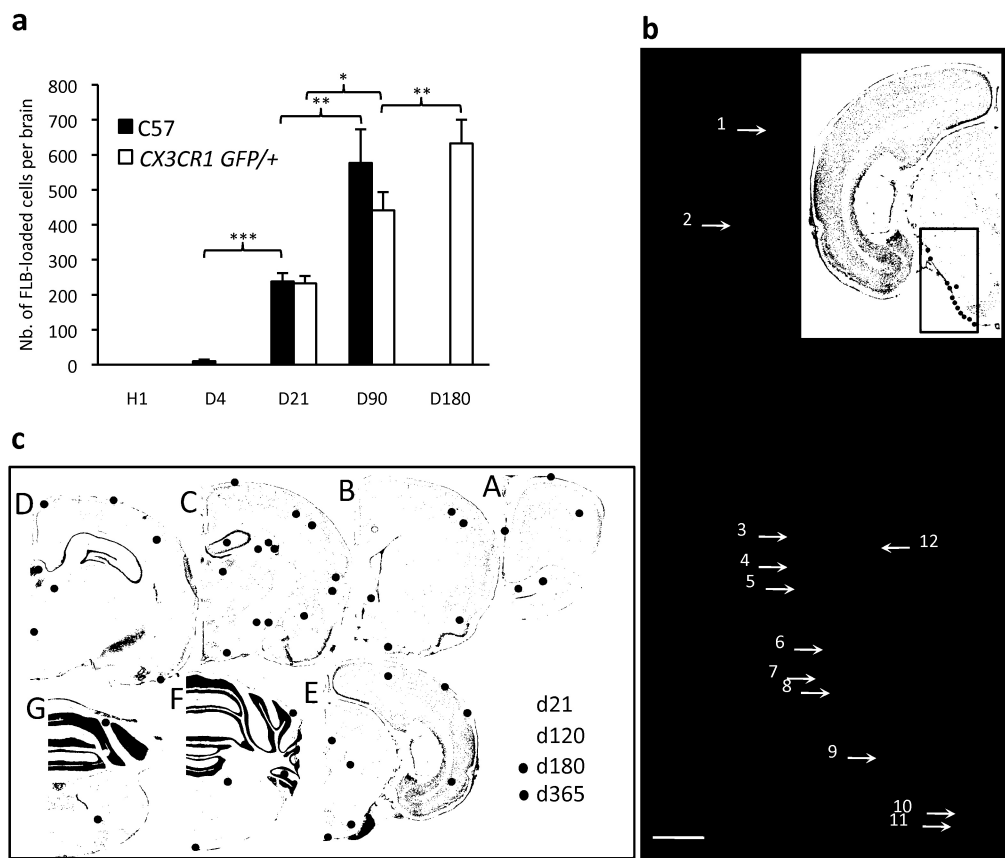


Figure 4

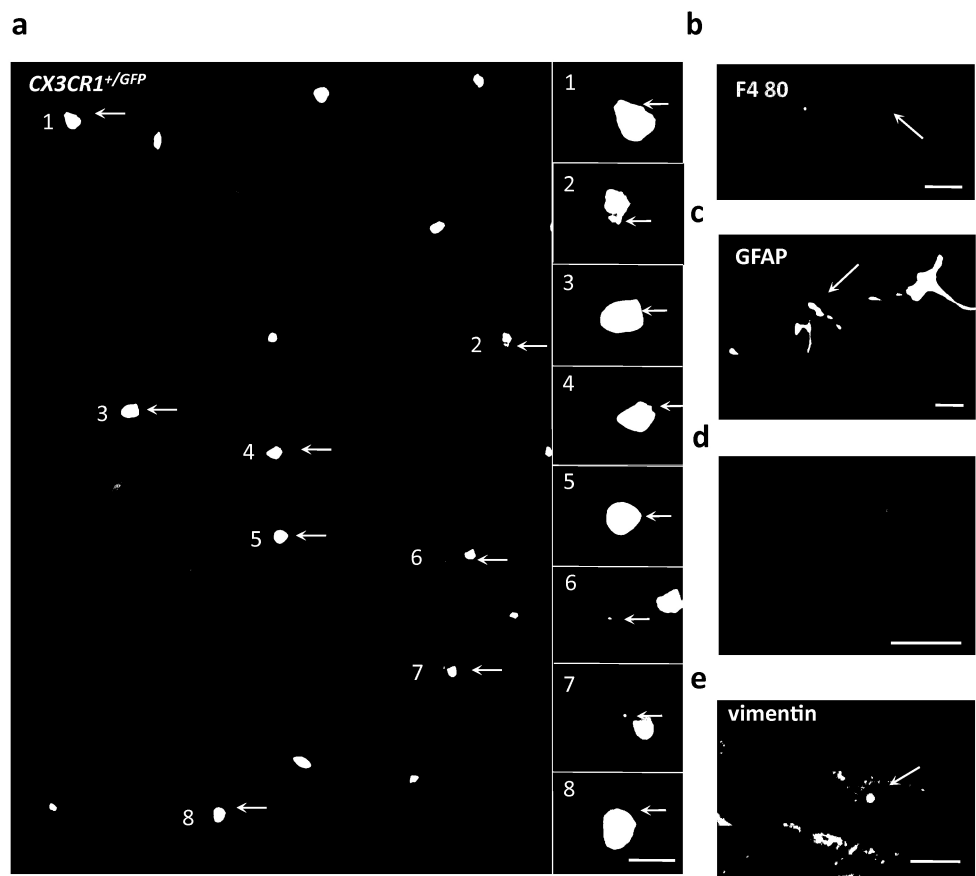


Figure 5

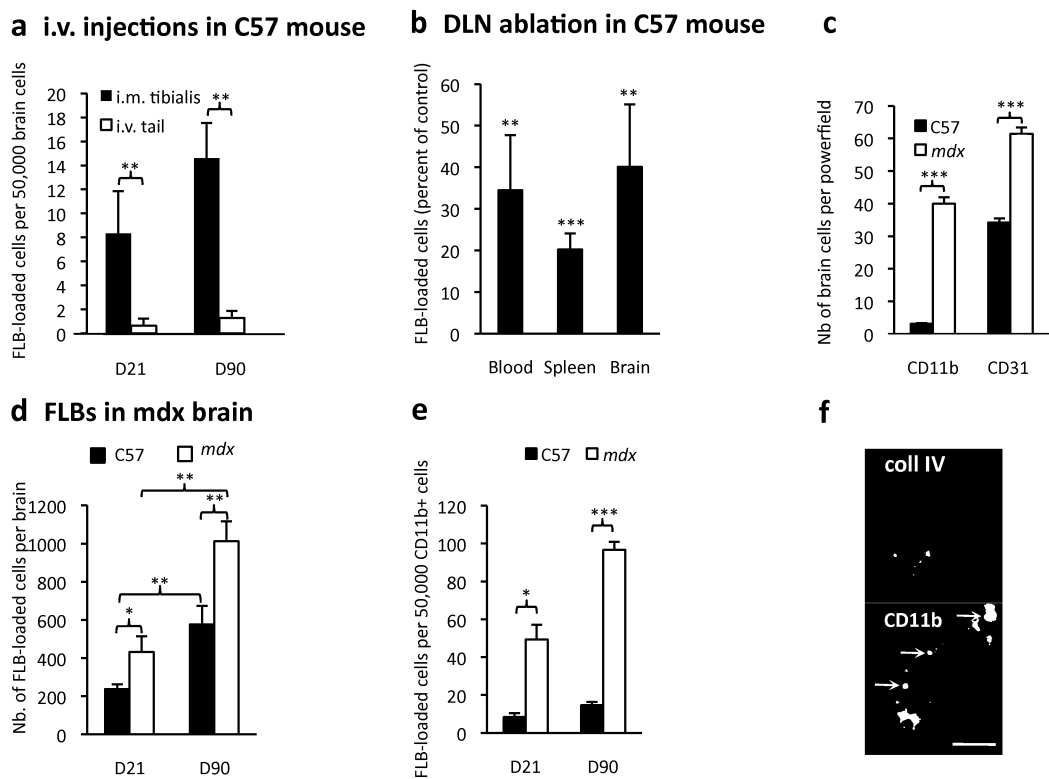


Figure 6

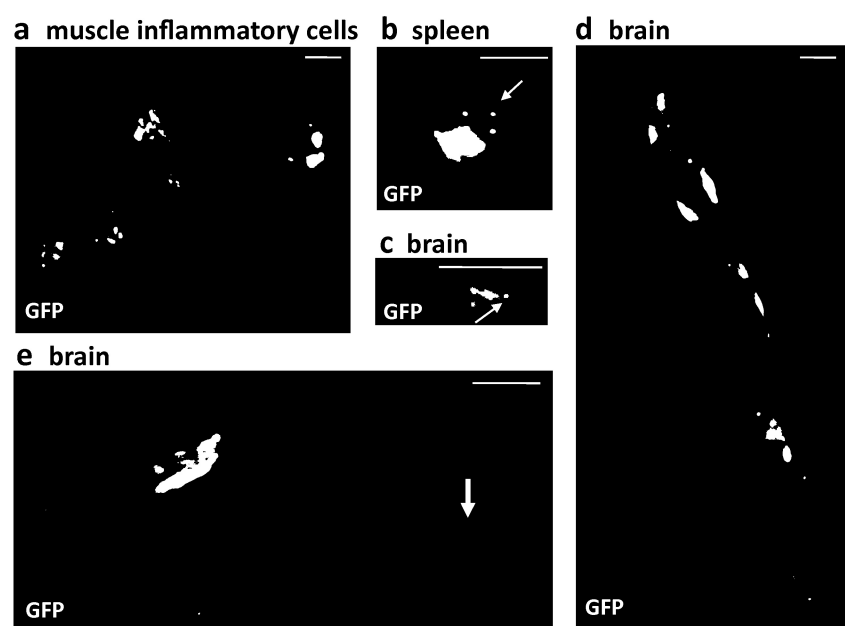


Figure 7

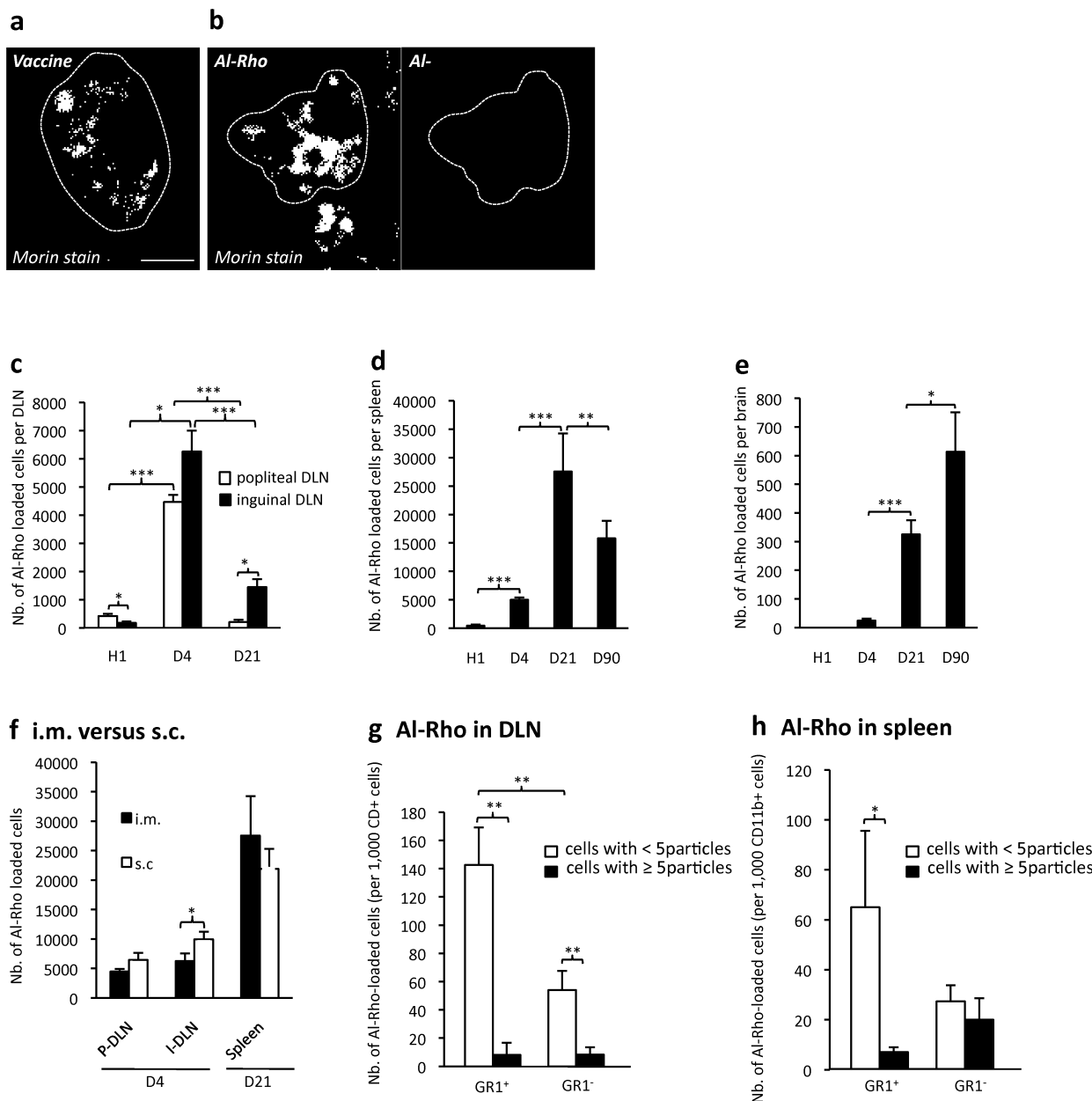


Figure 8

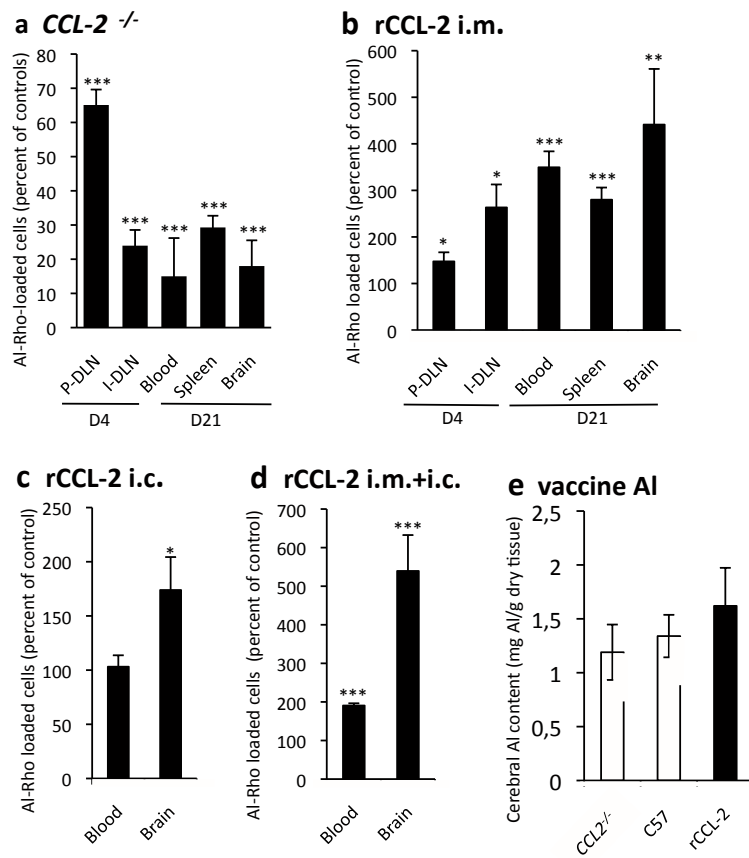


Figure 9

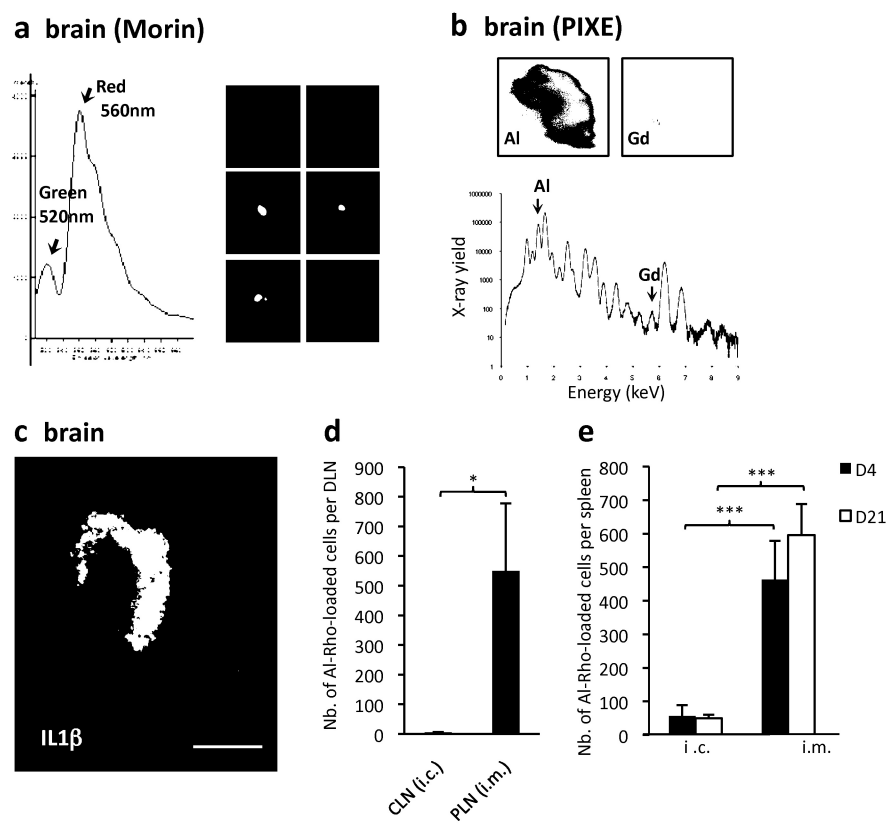


Figure 10

Additional files provided with this submission:

Additional file 1: Supplementary data BMC revised version.pdf, 159K
<http://www.biomedcentral.com/immedia/1817551102918215/supp1.pdf>